Spatial reactant distribution in CO_2 electrolysis: Balancing CO_2 utilization and Faradaic Efficiency

Siddhartha Subramanian, Joost Middelkoop and Thomas Burdyny*

Corresponding author email: T.E.Burdyny@tudelft.nl

Materials for Energy Conversion and Storage (MECS), Department of Chemical Engineering, Faculty of Applied Sciences, Delft University of Technology, van der Maasweg 9, 2629 HZ Delft, The Netherlands.

Abstract:

The production of value added C1 and C2 compounds within CO_2 electrolyzers has reached sufficient catalytic performance that system and process performance – such as CO_2 utilization – have come more into consideration. Efforts to assess the limitations of CO_2 conversion and crossover within electrochemical systems have been performed, providing valuable information to position CO_2 electrolyzers within a larger process. Currently missing, however, is a clear elucidation of the inevitable trade-offs that exist between CO_2 utilization and electrolyzer performance, specifically how the Faradaic Efficiency of a system varies with CO_2 availability. Such information is needed to properly assess the viability of the technology. In this work, we provide a combined experimental and 3D modelling assessment of the trade-offs between CO_2 utilization and selectivity at 200 mA/cm^2 within a membrane-electrode assembly CO_2 electrolyzer. Using varying inlet flow rates we demonstrate that the variation in spatial concentration of CO_2 leads to spatial variations in Faradaic Efficiency that cannot be captured using common 'black box' measurement procedures. Specifically, losses of Faradaic efficiency are observed to occur even at incomplete CO_2 consumption (80%). Modelling of the gas channel and diffusion layers indicated at least a portion of the H_2 generated is considered as avoidable by proper flow field design and modification. The combined work allows for a spatially resolved interpretation of product selectivity occurring inside the reactor, providing the foundation for design rules in balancing CO_2 utilization and device performance in both lab and scaled applications.

Introduction

One of the emerging technologies to mitigate fossil fuel-based carbon emissions is the electrochemical conversion of CO_2 to fuels and value-added products. In electrochemical CO_2 reduction, an electric potential is applied in the presence of an appropriate catalyst to convert CO_2 and H_2O to syngas ($CO+H_2$), ethylene (C_2H_4), ethanol (C_2H_5OH) and formate ($HCOOH$) among other products [1-4]. To meaningfully mitigate CO_2 emissions and be cost-competitive with alternative production routes, CO_2 electrolyzers will need to be proven as scalable to global production rates on the order of 100's Mtons/year [5-7]. While water electrolyzers are developmentally able to reach such scales, CO_2 electrolyzers are at a much earlier stage of development. Thus, while producing an anthropogenic carbon cycle composed of converting atmospheric CO_2 to fuels using solar and other renewable energy sources is appealing, additional research and development is needed to improve the performance metrics and scale of the technology for it to become a viable option [8-10].

To perform research into CO_2 electrolyzers at increased production rates, a greater fraction of research has taken place under elevated current densities (>100 mA/cm^2), using either high pressure systems or gas diffusion electrodes to enhance the availability of CO_2 at the catalyst surface. Gas diffusion electrodes (GDE) in particular have been found to be promising due to their ease of operation at atmospheric conditions which lowers the barrier for research to adopt their use [11-13]. When paired with novel catalyst architectures and cell designs, CO_2 electrolysis on GDE's has then achieved current densities on the order of 1A/cm^2 for promising products such as both CO [14] and ethylene [15] with reasonable faradaic efficiencies and cell voltages. Additionally, some researchers have begun discussing the importance of CO_2 utilization (as known as single-pass conversion efficiency) within such systems. Separate works have assessed the maximum conversion for a given configuration,[16] the crossover of the CO_2 to the anode as carbonate, [17] and the observed drop in faradaic efficiency at higher CO_2 utilizations [18]. Such research has made it clear that trade-offs will ultimately exist between the traditional performance metrics of the CO_2 electrolyzer itself (current density, Faradaic efficiency, overpotential), and the efficiency and cost of the entire CO_2 conversion process consisting of upstream and downstream processes [19].

The balance between CO_2 utilization and faradaic efficiency is particularly interesting as these metrics are directly impacted by the gas flow rate, the applied current density, temperature and the electrolyte alkalinity, all of which affect the CO_2 that is available for conversion. For example, Jeng at al.[16] highlighted the trade-off between partial current density for CO and the fraction of CO_2 converted to products for a 25 cm^2 membrane-electrode assembly (MEA) CO_2 electrolyzer under various operating conditions, noting a consistent maximum CO_2 utilization of 43% for the given reaction. While such observations provide valuable information around CO_2 utilization in such systems, the trade-off in faradaic efficiency with CO_2 utilization under varying CO_2 concentrations has received less attention and is less well-described. Specifically, while the CO_2RR faradaic efficiency of a system under excess

flow conditions can be determined using either a high gas flow rate or a very small geometric surface area (e.g. <1 cm^2), the selectivity of the system under decreasing CO_2 partial pressures is less clear with only a few studies available [20]. Importantly, as the surface area of standard test cells increases, *the concentration of CO_2 will also vary spatially throughout the reactor*, leading to spatial differences in reactivity and faradaic efficiency that will need to be understood to scale-up and optimize the technology.

While the influence of spatial reactant distribution on performance has not been well-investigated in the CO_2 electrolysis community, there is a wealth of research in the fuel cell community assessing the influence of reactant concentrations, flow patterning and under-rib convection on efficiency, utilization and mass transport on the overall performance of the device [21-24]. Using previous electrochemical fields as a guidepost, it is apparent that understanding the spatial variation of selectivity within a CO_2 electrolyzer device will also be an essential step towards scaling-up such devices as well as choosing configurations which maximize CO_2 utilization without unnecessary penalties in selectivity. For CO_2 electrolysis, these efforts are complicated by competing and homogenous reactions which poses additional challenges as compared to well-studied parallel electrochemical fields. There is also less data presently available evaluating the performance differences between different flow fields for the gaseous CO_2 channel as most research is performed using smaller geometric catalyst areas and a fully open cavity.

Here we sought to provide a framework for how reactant flowrate and spatial CO_2 distribution impacts product selectivity at higher CO_2 utilizations using a well-utilized electrochemical testing platform. Firstly, we performed CO_2 electrolysis using a silver (Ag) gas diffusion electrode in a 5 cm^2 MEA at various reactant flowrates to determine the macroscopic influence on product selectivity. From these experiments a 'black box' evaluation of faradaic efficiencies (FE) at various CO_2 utilizations is defined. We then built a 3D mass transport model of the cathode side of the MEA to estimate the spatial CO_2 distribution inside the reactor and catalyst layer under each of the varying flow conditions to convert the 'black box' results of the CO_2 distribution throughout the 5 cm^2 cell into a more spatially resolved interpretation of reactant concentration at the catalyst's surface (Fig.1). Finally, we show that by using a combined experimental and modelling approach, the influence of reactant flowrate and spatial CO_2 distribution can in turn be used to predict a spatial product selectivity across the device. Once defined, such a combined experimental and modelling system can then be used to predict the impacts of varying flow fields, cell areas and current densities, providing the groundwork for designing and prototyping CO_2 electrolyzers which balance CO_2 utilization with product selectivity.

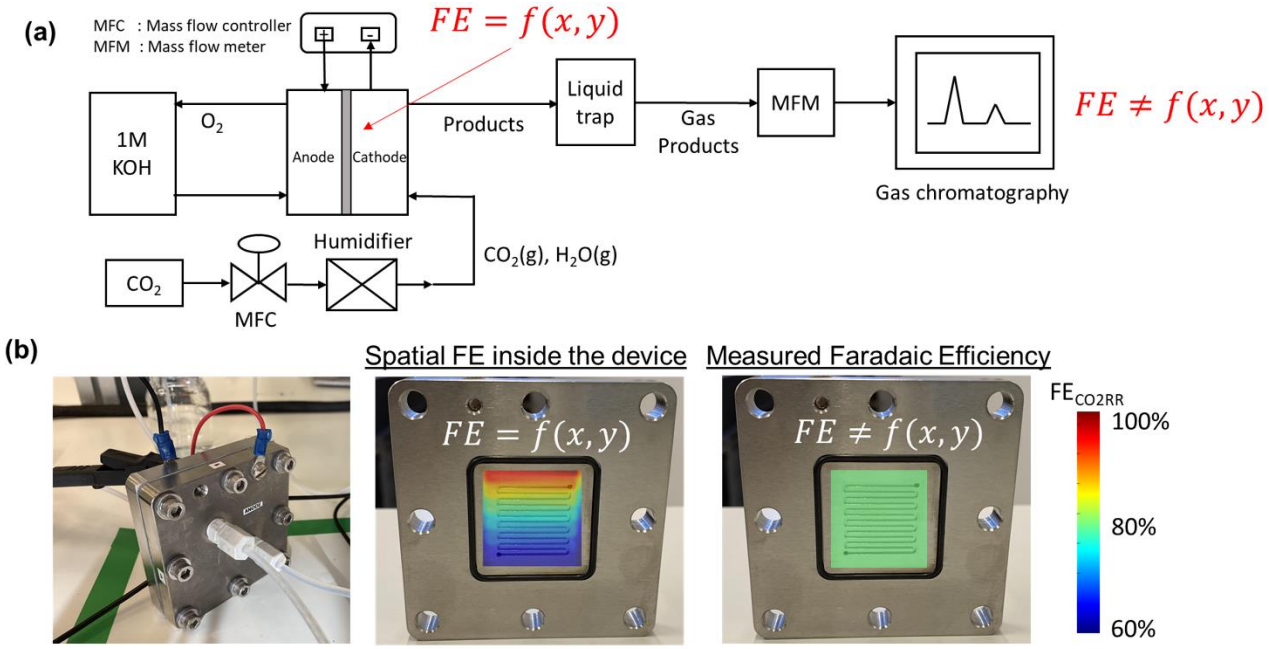

Fig. 1. (a) Simplified schematic of the experimental setup used for CO_2 electroreduction to CO in a membrane electrode assembly (MEA). (b) Figure of the experimental MEA utilized in the work. (c) Overlaid schematic of the actual vs measured Faradaic Efficiency of a CO_2 electrolysis system under CO_2-limited operating flow rates for the serpentine flow fields used for CO_2 flow behind a gas-diffusion layer.

Results and discussion

Product quantification within gaseous-fed CO_2 electrolyzers is presently performed by measuring the composition of the outlet gas phase using a gas chromatography (GC), and measuring the composition of the liquid electrolyte phases using nuclear magnetic resonance spectroscopy (NMR) or high performance liquid chromatography (HPLC). Such measurements provide a point-in-time 'black box' interpretation of the FE at a given flow rate, current density and configuration that can be monitored through periodic measurements (Fig. 1a). At elevated inlet flow rates where CO_2 utilizations are low, the outlet gas stream remains > 90% CO_2 and it is subsequently assumed that ample CO_2 can reach the entire catalytic surface area. In other words, no specific area of the catalyst surface exhibits mass transport limitations and the Faradaic Efficiency is assumed to be equal across the entire catalyst area (e.g. FE $\neq f(x,y)$). Such an assumption is particularly valid for smaller catalyst areas, high CO_2 flow rates and open cavity gas channels which are assumed as well-mixed and maintained at similar temperature and pressures.

As industrial and lab geometric cell areas increase, CO_2 must be distributed to the GDL and catalyst area through flow fields, which are also critically acting as a current collector to ensure homogenous electrode potentials. Within these CO_2 flow channels, the reactant and product compositions will then change along the length of each flow channel [25] as the catalyst consumes CO_2 and produces products such as CO and H_2. In cases where CO_2 utilizations are increased, spatial variations in performance and

selectivity will occur when areas of the catalyst no longer have access to sufficient CO_2, and produce unwanted H_2 instead (see Fig. 1b for representation) [26-28]. To begin assessing this trade-off we first collected a data set under varying flow rate conditions for CO_2 conversion to carbon-monoxide (CO) on a silver (Ag) catalyst in a membrane-electrode assembly with a serpentine flow field of 5 cm^2 geometric area (Fig. S2).

For the data set we performed electrolysis at a constant current density of 200 mA/cm^2 for 3600 seconds at inlet CO_2 flowrates between 10 and 50 sccm. The gas products and unreacted CO_2 were quantified using a mass-flow metre (MFM) and GC installed at the exit of the reactor (Fig. 1a)). As shown in Fig. 2a, we found that at excess flow rates between 20 and 50 sccm the Faradaic efficiency of CO_2 reduction products (CO and formate) was maintained between 93-97%, indicating that sufficient reactant is available throughout the system. At lower flow rates (<20 sccm), however the FE of hydrogen begins increasing steadily with increasing CO_2 utilization, reaching an H_2 selectivity of 38.9 % at 10 sccm and a measured CO_2 utilization of ~50 % (Fig. 2b). Over the entire examined region, CO_2 utilization decreases with an increase in the inlet flowrate from 50.8 % at 10 sccm to 16.8 % at 50 sccm as shown in Fig. 2b. The highlighted grey region in Fig. 2a and 2b represents the likely operating region of a commercial CO_2 electrolyzer as it best balances selectivity and utilization. Understanding and quantifying the performance trade-off is necessary to manufacture performance curves for CO_2 electrolyzers, similar to other applications where trade-offs exist (e.g. centrifugal pumps). Such data is essential for positioning CO_2 electrolyzers within integrated process and cost models that assess a broad operational parameter space. Additionally, better design of the reactant flow fields and gas-diffusion layers may improve performance further.

To better quantify the trade-off in utilization and selectivity, the available CO_2 for reduction in the system must be known. To track this a carbon balance of the system is performed at various flow rates (Fig. 2c). In this analysis the inlet and outlet flow rates of CO_2, CO and formate are all measured directly, with the exception of CO_2 crossing the membrane as carbonate ions which was assumed to complete the carbon balance. Observing the trends in carbon flow rates, two interesting points arise. First, even under low flow rates of 10 sccm, some CO_2 is observed in the outlet of the reactor (~5% /v) even though the reaction appears CO_2-limited. This indicates a measure of transport limitations between the serpentine gas channel and the catalyst's surface as a result of transport through the gas-diffusion media and into the catalyst layer. And second, the consumption of CO_2 by OH^- ions is non-linear and varies with the availability of CO_2 throughout the reactor. Both of these observations can be qualitatively interpreted from the presented data, but lack a quantitative interpretation in their present form as a result of the 'black box' measurement approach. Thus, a numerical transport model built upon the experimental results can be used to provide further understanding.

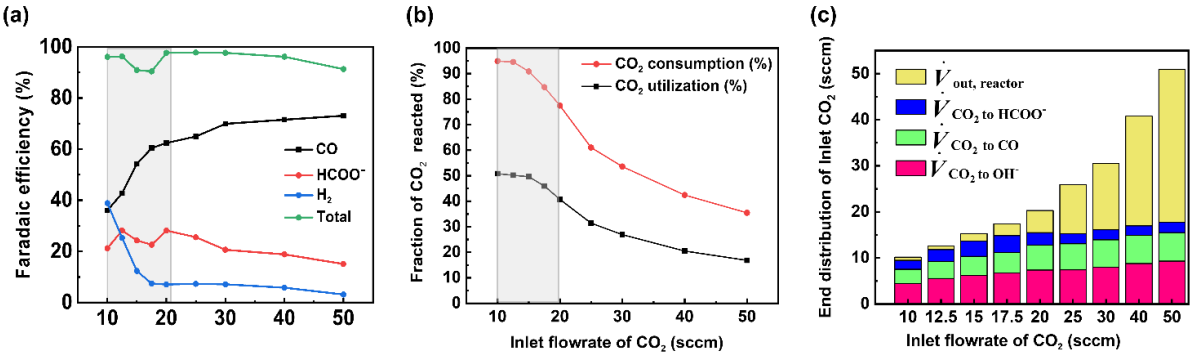

Fig. 2. (a) Faradaic efficiency of products for various inlet flow rates performed at a current density of 200 mA/cm^2. CO_2 utilization and CO_2 consumption for different inlet flowrates at 200 mA/cm^2. Greyed regions represent trade-offs between utilization and selectivity. (c) Carbon balance on cathode showing the volumetric flowrate of CO_2 consumed to different reactions.

Modelling CO_2 Spatial Distribution

To gain deeper understanding of the reactant distribution inside the reactor, a 3D model of the mass transport and fluid flow in the cathode compartment of the MEA cell was created using COMSOL Multiphysics (Fig. 3a). The ultimate goal of the model is to provide a simple estimate of the concentration of CO_2 at the surface of the catalyst layer for various operating conditions, which can then be used to predict a spatial and average Faradaic efficiency ($FE = f(x,y)$ and $FE_{average}$). The predicted average FE of the system in particular provides a comparison to the experimental data, while the spatial assessment is useful to advance performance further and for the design of scaled systems beyond 5 cm^2.

Included within the model are the CO_2 serpentine gas channel and a gas-diffusion layer composed of a carbon fibre backing and a microporous layer (Fig. S6). The gas-diffusion electrode is then modelled as a porous media similar to other works [29] . In the model an inlet flux of CO_2 is provided to the system in the gas channel, while a fixed current density is imposed at the surface of the gas-diffusion electrode to model the electrochemical reactions and consumption of CO_2 by the electrolyte. The physical parameters and properties used in the model are shown in Table S5.

Due to the complexity of constructing a fully-representative macroscopic and nanoscopic transport model, we have chosen to set our system boundaries at the interface of the microporous layer and the catalyst layer. The model then does not directly take into account the interaction between the catalyst layer and the membrane, 3D transport effects within the nanopores of the catalyst layer, or the homogenous $CO_2/HCO_3^-/CO_3^{2-}$ reactions occurring within the liquid water and Sustainion membrane. To account for this we have constructed three modelling scenarios using experimental mass flows as inputs to construct different empirical models that highlight the effect of different scenarios on CO_2 distribution. The most representative system is then used to continue the discussion on CO_2 utilization and Faradaic Efficiency.

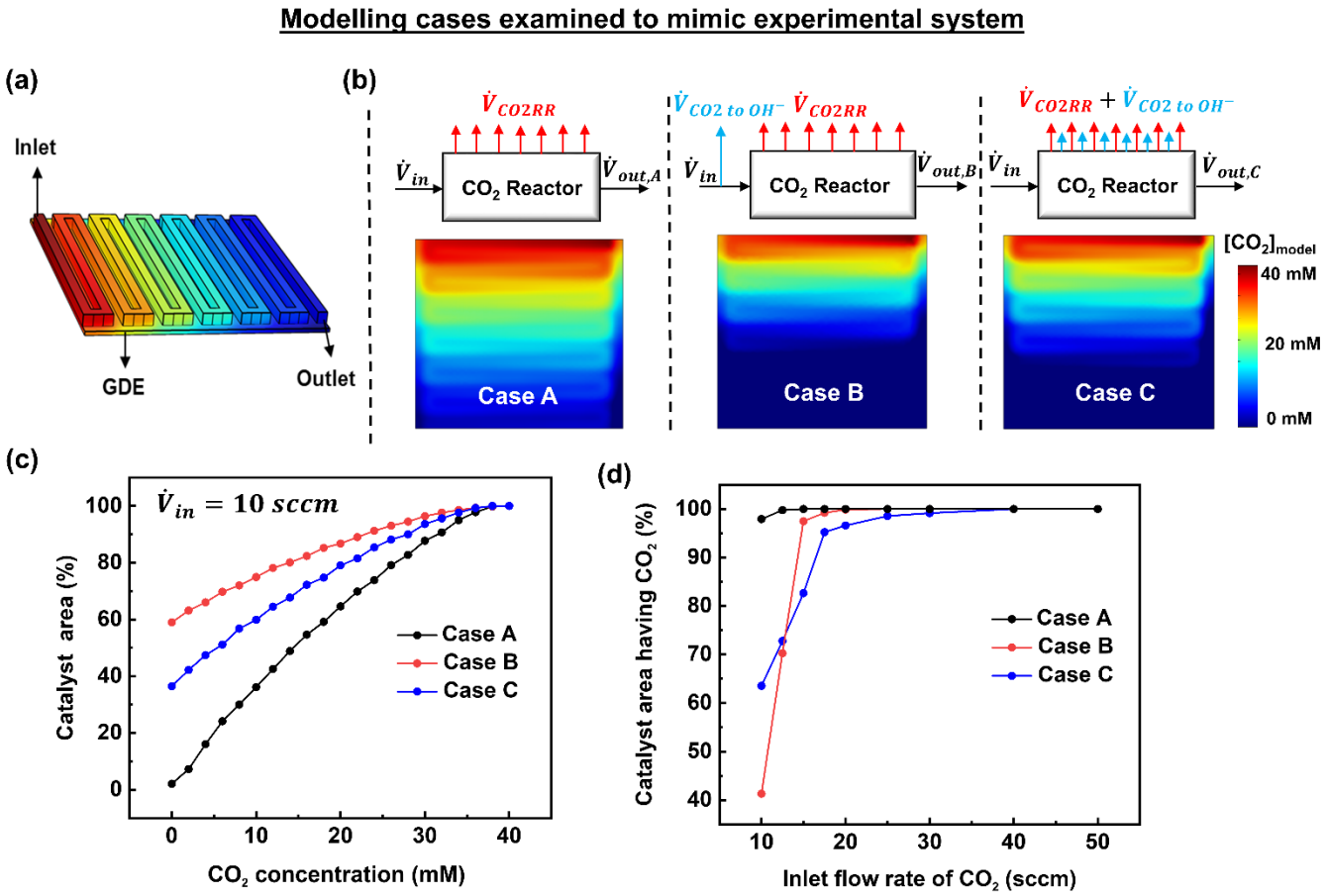

Fig.3 (a) 3D model of the flow channel and gas diffusion electrode. (b) Modelling cases examined to mimic the experimental observations. Shown here are the simulation results of CO_2 concentration at the catalyst surface for an inlet flow rate of 10 sccm and 200 mA/cm^2, (c) A cumulative distribution plot for the three cases showing the [CO_2] distribution at the catalyst surface, (d) Portion of catalyst surface having access to CO_2 ([CO_2] > 0) for all the inlet flow rates studied experimentally.

The three examined cases are as follows: In Case A, we ignore the fraction of CO_2 reacting with hydroxide ions. In Case B, the amount of CO_2 lost to hydroxide ions is subtracted at the inlet resulting in a reduced inlet flowrate. In Case C, the fraction of CO_2 lost to hydroxide ions is assumed to occur homogenously throughout the catalyst surface. These three cases are visually depicted in Fig. 3b along with their resulting simulated CO_2 concentrations at the catalyst layer interface at 10 sccm and 200 mA/cm^2. Fig. 3c shows the analysed data set from Fig. 3b represented as a cumulative distribution function for the percentage of the catalyst area with a minimum concentration of CO_2.

Case A : Modelling the cathode without accounting for CO_2 reacting with OH^- ions

In this approach, CO_2 losses due to its reaction with OH^- ions forming bicarbonate and carbonate ions are ignored. The results obtained for an inlet flowrate of 10 sccm at 200 mA/cm^2 are shown in Fig. 3c, where the two-dimensional data set has been converted into a cumulative distribution functions as a percentage of the geometric area of the catalyst layer. Thus the percentage of catalyst area with ample

and deficient CO_2 can be visualized (Fig.S8). From Fig. 3b it can be seen that the CO_2 concentration decreases from the inlet to the outlet of the gas channels and at the catalyst surface. As shown in Fig.3b, the cumulative distribution plot for CO_2 at the catalyst surface shows that only 2.1 % of the catalyst area is deficit of CO_2 for an inlet flow rate of 10 sccm. Hence, Case A shows almost no CO_2 limitation indicating that this reactant feed is sufficient to sustain the current density that is applied (200 mA/cm^2). However, as could be expected, Case A clashes with the experimental observation of a low CO selectivity (35.9 %) and a relatively high H_2 selectivity (38.9%) at 10 sccm. This discrepancy between the modelling and the experimental results shows that CO_2 losses (due to its reaction with OH^-) cannot be ignored in modelling the spatial CO_2 distribution.

Case B: Modified inlet flow rate approach

In Case B the inlet boundary condition of CO_2 flux has been reduced to account for the amount of CO_2 lost to OH^- ions over the entire reactor. Here, the amount of CO_2 lost to OH^- ions was experimentally measured and subtracted from the inlet flow rate to obtain a modified inlet flow rate (Table S2). In contrast to Case A, using the modified inlet flow rate approach a significant portion of catalyst surface (59 %) is deficit of CO_2 at 10 sccm (Fig. 3b). Although this agrees with the experimental observation of an increased H_2 production (38.9 %) at low flow rates, the change in catalyst area with access to CO_2 is too abrupt under varied flow rates (Fig. 3d), which does not pair well with the gradual change in selectivity seen in the experiments (Fig. 2a). The flaw in a modified inlet flow rate approach is that the CO_2 losses to OH^- ions are not distributed throughout the catalyst surface, meaning that the CO_2 available in the front half of the serpentine channel is unfairly limited. Case B is then too much of a simplification to predict the spatial CO_2 distribution and device selectivity accurately.

Of note, using a modified inlet flow rate would also slightly impact the fluid velocity and pressure drop between the inlet and outlet, altering the actual physical phenomena occurring inside the reactor. Such an approach would then have significant effects when large flow rates are used where a significant pressure drop might exist between the inlet and outlet of the reactor. Critically, Case B over penalizes the CO_2 concentration throughout the majority of the reactor as CO_2 lost to OH^- near the exit of the reactor has been removed prior to the reactor inlet.

Case C: Modified current density approach (Modified CO_2 flux to the catalyst)

With the aim of predicting the 2D spatial CO_2 concentration in the reactor while maintaining a simplified modelling approach, Case C aimed to spatially account for CO_2 loss to OH^- as well. To institute this within the model without implementing pore scale phenomena and homogeneous reactions, we instead imposed a penalty current density (j_{loss}) that accounts for the additional consumption of CO_2. The magnitude of the imposed penalty current density was calculated using the experimentally-measured loss of CO_2 at each independent flow rate (Eq. 1 and Fig. 2c), resulting in an empirical representation of the experiment. This modified current density was then added to the actual

applied current density term to provide the spatial rate of CO_2 consumption (Eq. 2). Fig. S3 shows the modified current densities which have been imposed in the model as a result of Case C, with all current density above 200 mA/cm^2 being deployed as a non-Faradaic consumption of CO_2.

$$j_{loss} = \frac{n^e \times n_{CO2\ to\ OH-} \times F}{A} \quad (1)$$

$$R_{CO2} = \frac{(j_{applied} + j_{loss})}{n^e F} \quad (2)$$

Here, R_{CO2} is the reaction rate of CO_2, j_{loss} is the modified current density calculated based on the amount of CO_2 lost to OH^- ions (from experimental data), n^e is the number of electrons (2 for CO_2 RR), $n_{CO2\ to\ OH-}$ is the moles of CO_2 lost to OH^-, F- Faraday's constant and A is the area of the catalyst surface (6.25 cm^2).

Once imposed, Case C provides the spatial distribution of CO_2 observed in Fig. 3b for an inlet flow rate of 10 sccm. Translating this to the cumulative distribution function in Fig. 3c, the net catalyst area with no access to CO_2 is approximately 37%. Further, Fig. 3d shows the percentage of catalyst area with access to reagent results for all of the simulated cases and flow rates. Notably at flow rates within the utilization area of interest (10-20 sccm), Case C falls in between Cases A and B. The effect of parasitic CO_2 loss is still not eliminated above 20 sccm, however, which can be attributed to poor CO_2 access on the fringes of the gas-diffusion layer. In this case, this is due to the area of the GDE (6.25 cm^2) expanding beyond the edge of the serpentine flow channel (5 cm^2). Due to accounting for spatial effects, Case C is chosen as the most representative model for the remainder of the work.

Predicted spatial and average Faradaic efficiency

The previous section provided a set of models to predict the spatial concentration of CO_2 within an experimentally-tested membrane-electrode assembly reactor. As the primary focus is to better understand the trade-offs between selectivity and utilization in these systems, these predicted concentrations of CO_2 must be translated to a predicted spatial and average Faradaic Efficiency. To accomplish this we imposed the following selectivity criteria in equations 3 and 4 based upon the predicted CO_2 concentration, and the experimentally-measured Faradaic Efficiency under an excess CO_2 flow rate of 50 sccm (97% CO_2RR / 3% HER). The data has been normalized to 100% (96.8% CO_2RR / 3.2% HER) for the purposes of the model.

$$FE_{CO2RR}(x,y) = \begin{cases} 96.8\%, & [CO_2] > 0 \\ 0\%, & [CO_2] = 0 \end{cases} \quad (3)$$

$$FE_{H_2}(x,y) = \begin{cases} 3.2\%, & [CO_2] > 0 \\ 100\%, & [CO_2] = 0 \end{cases} \quad (4)$$

Using this criteria, the spatial Faradaic Efficiency across the catalyst layer of the GDE is visually shown in Fig. 4a for three different flow rates. Observing the low flow rate case of 10 sccm, the loss of selectivity towards CO_2RR is shown to be primarily due to insufficient CO_2 along the length of the reactor towards the outlet. In the 20 sccm case, however, it is only the edges near the outlet of the reactor that are expected to primarily produce H_2 instead of CO_2RR products. The plots in Fig. 4a for spatial selectivity are predicated on the assumption that there is not a transition region of selectivity between the shown blue and red regions. In an actual system the switch in selectivity from primarily CO_2RR to H_2 along the reactor of CO_2-deficient system would be more gradual, but high selectivities are known to be possible even at lower partial pressures [30]. A secondary check of the approach is to translate the spatially-predicted Faradaic Efficiency into a device-averaged FE like that reported experimentally.

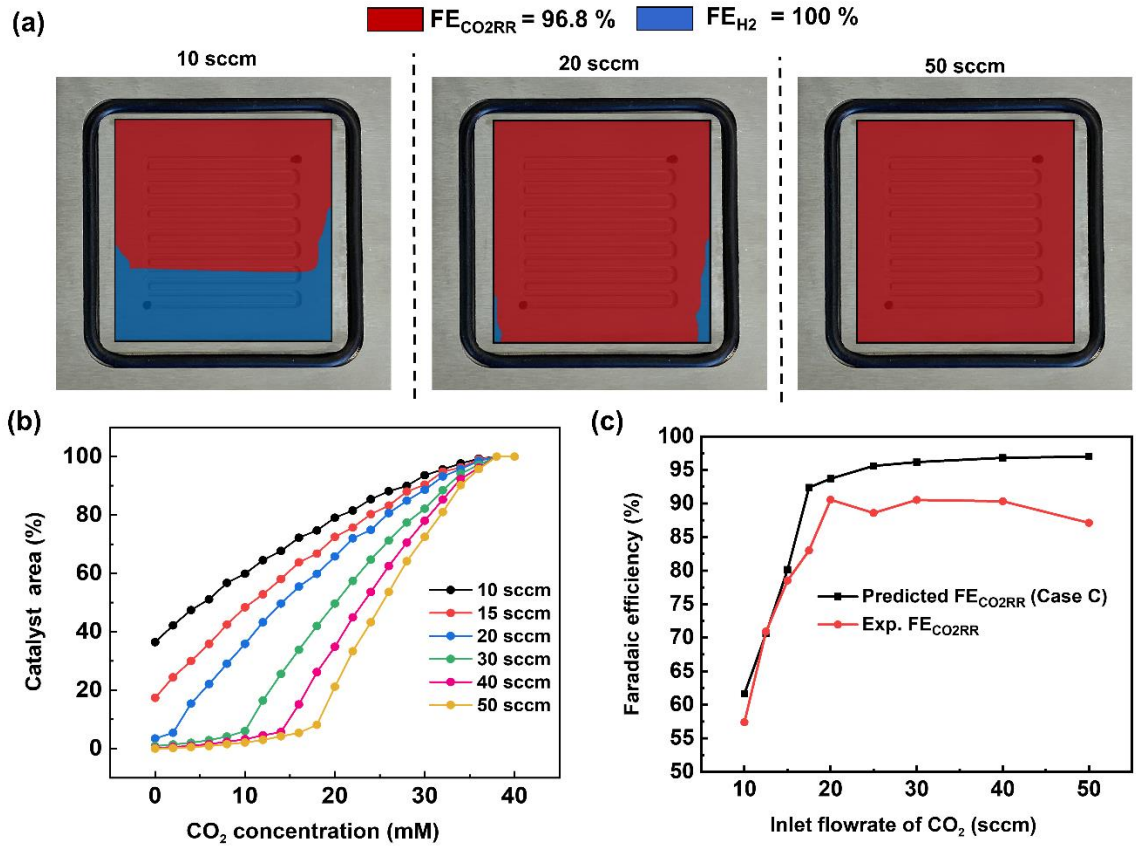

Fig.4. (a) CO_2 concentration map at the catalyst surface determined from the numerical simulations showing the spatial CO_2 distribution at various inlet flowrates, (b) A cumulative distribution plot of CO_2 concentration at the catalyst surface for different inlet CO_2 flow rates studied using a modified current density approach and (c) Comparison of predicted faradaic efficiency of CO_2RR with experimentally determined faradaic efficiency ($FE_{CO} + FE_{HCOO-}$).

The device-averaged FE can be calculated by using the distribution function in Fig. 4b for a variety of different flow rates, and combining this with the criteria presented in Eqs. 1 and 2. The resulting

predicted FE of CO_2RR and H_2 for all the inlet flowrates studied are then shown in Fig.4c, with the experimentally-measured values overlaid. It can be seen clearly that the predicted FE is in close agreement with the experimental FE of CO_2RR, showing the promise for using predicted CO_2 distribution within the reactor to predict spatial and average device selectivity. The consistent overprediction can be attributed to the experimental FE's being less than 100 %, most likely due to the inability to capture all produced formate in MEA cell. Importantly both the trend in selectivity within the higher CO_2 utilization region (10 to 20 sccm), as well as in the lower utilization range (20-50 sccm), follow the experimental data set well. Such a model forms the foundation for comparing GDE's with different permeability, flow fields with different geometries, and the trade-offs with selectivity and utilization under different current densities.

The model can also be used to draw new observations from the experimental data set. For example, the incremental change in CO_2RR from 20-50 sccm is shown to be due to a CO_2 deficiency on the outer edges of the domain where the larger gas-diffusion layer (6.25 cm^2) loses access to CO_2 from the 5 cm^2 serpentine channel area (see 20 sccm plot in Fig. 4a). Such an area then only produced H_2, which slightly lowers the "black box" measured FE via gas chromatography. We are then able to predict the location on the catalyst surface where CO_2 limitation occurs, which can help in understanding and designing flow channel designs at the cathode.

We also envisage that the water concentration at the catalyst surface (reaction interface) would always be > 0 and does not vary significantly based on the relative humidity measurements in our tests at the inlet and outlet of the reactor (R.H of 75% at inlet and 79% at outlet). This result is in agreement with a recent study on water quantification in a MEA where in-situ humidity measurements were performed during CO_2 electroreduction to confirm that the water concentration at the catalyst surface (membrane-GDE interface) remains constant regardless of the humidity level at the inlet CO_2 stream[29].

Finally, we emphasize here that at an applied current density of 200 mA/cm^2 , there is an increase in the amount of CO_2 reacting with OH^- ions with an increase in the reactant flow rate, which is identified in the increase in the j_{loss} value (Table S2). This is quite reasonable since the local OH^- ions generated at 200 mA/cm^2 is a constant (1.3 x10^{-5} mol/s) and an increase in the local CO_2 concentration due to increased inlet flowrate shifts the reaction to the right producing more HCO_3^- and CO_3^{2-} ions. Moreover, this reduction in local [OH^-] with increasing inlet flow rates would also reduce the local pH altering the reaction environment around the catalyst surface. A further increase in inlet flow rate (60-100 sccm) would result in the consumption of all the OH^- ions generated at the catalyst producing more HCO_3^- and CO_3^{2-} ions with a subsequent alteration of the local reaction environment. Operating at such high reactant flow rates would however reduce the CO_2 utilization to less than 10% and also increase the pressure drop between the inlet and outlet (serpentine channel) resulting in an increased pumping power [31]. Hence, optimizing the reactant flow rate to overcome CO_2 mass transport losses as well as

ensuring a high CO_2 utilization and a low pressure drop is a challenge. Therefore, we restricted our focus of this study to flow rates of up to 50 sccm.

Formate production from Ag GDE

While much of the work here focussed on the availability of CO_2 and the subsequent CO_2RR selectivity as a result of this, the experimental data set noted interesting and opposing trends in CO and formate selectivity under a variety of flow rate conditions (Fig. 2a). In particular while overall CO_2RR versus HER trended downward as flow rates decreased as could be expected (Fig. 5a), the selectivity of CO to formate also followed a similar linear trend, both within the CO_2-limited and non-limited flow rate regions (Fig, 5b). Here, we briefly contextualize these results and offer possible explanations given previous literature reports and our spatial model constructed here. It is worth noting that to measure formate we performed HPLC measurements of the anolyte samples post electrolysis for our Ag GDE system, meaning that only formed formate which crossed the anion exchange membrane could be measured, likely explaining some missing FE in our data set. We will provide speculation in spite of this.

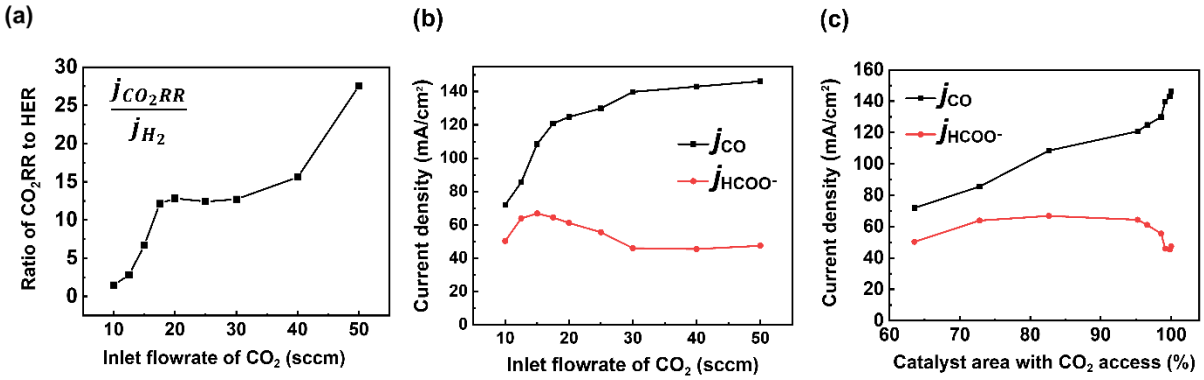

Fig. 5. (a) Ratio of partial current densities of CO_2 RR ($CO+HCOO^-$) and H_2. Partial current densities of CO and formate with **(b)** varying inlet CO_2 flowrates and **(c)** Catalyst area with CO_2 access.

The trend in CO to formate within the two flow rate regions have two possible explanations from literature: (i) the reaction pathway to formate exists through surface-adsorbed protons and competition with HER, (ii) formate selectivity supplants some CO selectivity under higher alkalinity conditions. The first point has been reported previously by Bohra et.al [32] using DFT calculations which showed that *OCHO towards formate forms through a bound *H, whereas CO formation proceeds first through direct CO_2 absorption. Thus, formate formation requires the Volmer step from HER formation in order to be formed. It would then be expected to see a lower CO/formate ratio when *H is more common, which would be the case in decreased and depleted CO_2 conditions like those observed from 10 to 20 sccm. Regarding (ii), previous studies on GDE flow cells have shown increased formate/CO ratios under extremely alkaline conditions (11 M KOH in Seifitokaldani et.al [33]) and decreased formate/CO ratios under higher CO_2 pressures (Gabardo et al. [34]). Both reports indicate that the pH of the reaction

environment will influence the ratio of CO to formate produced. Within our system, this hypothesis could help to explain the decreasing trend in formate production as the inlet flow rate ranges from 20-50 sccm. At higher flow rates excess CO_2 is available to negate the formed OH^- from the fixed current density reaction (see $V_{CO2\ to\ OH-}$ blocks in Fig. 2c). It is then likely that the reaction environment surrounding the catalyst layer leans to lower alkalinities at 50 sccm versus that of 20 sccm, even though ample CO_2 is available in both cases. The experimental decrease in j_{HCOO^-} is also seen when the model and experiments are combined (Fig.5c), where formate current density drops when the full catalyst area has access to CO_2.

Conclusion

The balance between CO_2 utilization and selectivity with electrochemical systems will be ever more important as CO_2 electrolyzers are scaled to larger areas and considered within larger chemical processes due to implications they have on reliability, separation processes and system costs. The trade-offs in these metrics are currently measured and reported for an entire reactor, while being driven by spatial variation in concentrations across an entire electrochemical reactor. At present, the experimental ability for direct localized measurement of CO_2 electrolysis products has not been demonstrated however. The work presented here aims to predict this trade-off by paring bulk product measurement with a transport model to provide a measure of spatial resolution to our electrochemical cell. We believe that our approach can provide a starting point for a more extensive modelling study to enhance the understanding of the local reaction environment around the catalyst surface in a membrane electrode assembly configuration, employing anion exchange membranes. Importantly, we hope this work inspires experts from adjacent fuel cell community to provide their wealth of experience to accelerate the CO_2 reduction field forward.

Author Contributions

S.S completed all of the experiments and modelling work. J.M. setup the experimental apparatus and assisted with experimental issues. T.B. and S.S. conceived the project. All authors contributed to writing and editing of the manuscript.

Conflicts of interest

There are no conflicts to declare.

Acknowledgements

Thomas Burdyny and Siddhartha Subramanian would like to acknowledge the co-financing provided by Shell and a PPP-allowance from Top Consortia for Knowledge and Innovation (TKI's) of the Ministry of Economic Affairs and Climate in the context of the TU Delft e-Refinery Institute. TB would also like to acknowledge the NWO for an individual Veni grant. The authors would also like to

acknowledge Mark Sassenburg for HPLC analysis and Sanjana Chandrasekar, Erdem Irtem and all members of Burdyny Energy lab for helpful discussions.

References

[1] Hori, Y. I. (2008). Electrochemical CO_2 reduction on metal electrodes. In *Modern aspects of electrochemistry* (pp. 89-189). Springer, New York, N Y.

[2] Tang, W., Peterson, A. A., Varela, A. S., Jovanov, Z. P., Bech, L., Durand, W. J., & Chorkendorff, I. (2012). The importance of surface morphology in controlling the selectivity of polycrystalline copper for CO_2 electroreduction. *Physical Chemistry Chemical Physics*, *14*(1), 76-81.

[3] Hori, Y., Takahashi, I., Koga, O., & Hoshi, N. (2002). Selective formation of C2 compounds from electrochemical reduction of CO_2 at a series of copper single crystal electrodes. *The Journal of Physical Chemistry B*, *106*(1), 15-17.

[4] Dinh, C. T., Burdyny, T., Kibria, M. G., Seifitokaldani, A., Gabardo, C. M., De Arquer, F. P. G., & Sargent, E. H. (2018). CO_2 electroreduction to ethylene via hydroxide-mediated copper catalysis at an abrupt interface. *Science*, *360*(6390), 783-787.

[5] Gao, D., Arán-Ais, R. M., Jeon, H. S., & Cuenya, B. R. (2019). Rational catalyst and electrolyte design for CO_2 electroreduction towards multicarbon products. *Nature Catalysis*, *2*(3), 198-210.

[6] Smith, W. A., Burdyny, T., Vermaas, D. A., & Geerlings, H. (2019). Pathways to industrial-scale fuel out of thin air from CO_2 electrolysis. *Joule*, *3*(8), 1822-1834.

[7] Sánchez, O. G., Birdja, Y. Y., Bulut, M., Vaes, J., Breugelmans, T., & Pant, D. (2019). Recent advances in industrial CO_2 electroreduction. *Current Opinion in Green and Sustainable Chemistry*, *16*, 47-56.

[8] Burdyny, T., & Smith, W. A. (2019). CO_2 reduction on gas-diffusion electrodes and why catalytic performance must be assessed at commercially-relevant conditions. *Energy&Environmental Science*, *12*(5), 1442-1453.

[9] Kibria, M. G., Edwards, J. P., Gabardo, C. M., Dinh, C. T., Seifitokaldani, A., Sinton, D., & Sargent, E.H.(2019). Electrochemical CO2 reduction into chemical feedstocks: from mechanistic electrocatalysis models to system design. *Advanced Materials*, *31*(31), 1807166.

[10] Larrazábal, G. O., Martín, A. J., & Perez-Ramirez, J. (2017). Building blocks for high performance in electrocatalytic CO_2 reduction: materials, optimization strategies, and device engineering. *The journal of physical chemistry letters*, *8*(16), 3933-3944.

[11] Ma, S., & Kenis, P. J. (2013). Electrochemical conversion of CO_2 to useful chemicals: current status, remaining challenges, and future opportunities. *Current Opinion in Chemical Engineering*, *2*(2), 191-199.

[12] Higgins, D., Hahn, C., Xiang, C., Jaramillo, T.F. and Weber, A.Z., 2018. Gas-diffusion electrodes for carbon dioxide reduction: a new paradigm. *ACS Energy Letters*, *4*(1), 317-324.

[13] Whipple, D. T., Finke, E. C., & Kenis, P. J. (2010). Microfluidic reactor for the electrochemical reduction of carbon dioxide: the effect of pH. *Electrochemical and Solid State Letters*, *13*(9), B109.

[14] Endrődi, B., Kecsenovity, E., Samu, A., Halmágyi, T., Rojas-Carbonell, S., Wang, L., ... & Janáky, C. (2020). High carbonate ion conductance of a robust PiperION membrane allows industrial current density and conversion in a zero-gap carbon dioxide electrolyzer cell. *Energy & Environmental Science*, *13*(11), 4098-4105.

[15] De Arquer, F. P. G., Dinh, C. T., Ozden, A., Wicks, J., McCallum, C., Kirmani, A. R., & Sargent, E. H. (2020). CO_2 electrolysis to multicarbon products at activities greater than 1 A cm^{-2} *Science*, *367*(6478), 661-666.

[16] Jeng, E., & Jiao, F. (2020). Investigation of CO_2 single-pass conversion in a flow electrolyzer. *Reaction Chemistry & Engineering*, *5*(9), 1768-1775.

[17] Ma, M., Clark, E. L., Therkildsen, K. T., Dalsgaard, S., Chorkendorff, I., & Seger, B. (2020). Insights into the carbon balance for CO_2 electroreduction on Cu using gas diffusion electrode reactor designs. *Energy & Environmental Science*, *13*(3), 977-985.

[18] Gabardo, C.M., O'Brien, C.P., Edwards, J.P., McCallum, C., Xu, Y., Dinh, C.T., Li, J., Sargent, E.H. and Sinton, D., 2019. Continuous carbon dioxide electroreduction to concentrated multi- carbon products using a membrane electrode assembly. *Joule*, *3*(11), 2777-2791.

[19] Smith, W. A., Burdyny, T., Vermaas, D. A., & Geerlings, H. (2019). Pathways to industrial-scale fuel out of thin air from CO_2 electrolysis. *Joule*, *3*(8), 1822-1834.

[20] Kyriacou, G. Z., & Anagnostopoulos, A. K. (1993). Influence CO_2 partial pressure and the supporting electrolyte cation on the product distribution in CO_2 electroreduction. *Journal of applied electrochemistry*, *23*(5), 483-486.

[21] Dutta, S., Shimpalee, S., & Van Zee, J. W. (2000). Three-dimensional numerical simulation of straight channel PEM fuel cells. *Journal of Applied Electrochemistry*, *30*(2), 135-146.

[22] Futerko, P., & Hsing, I. M. (2000). Two-dimensional finite-element method study of the resistance of membranes in polymer electrolyte fuel cells. *Electrochimica Acta*, *45*(11), 1741-1751.

[23] Wang, Z. H., Wang, C. Y., & Chen, K. S. (2001). Two-phase flow and transport in the air cathode of proton exchange membrane fuel cells. *Journal of power sources*, *94*(1), 40-50.

[24] Nam, J. H., Lee, K. J., Sohn, S., & Kim, C. J. (2009). Multi-pass serpentine flow-fields to enhance under-rib convection in polymer electrolyte membrane fuel cells: Design and geometrical characterization. *Journal of Power Sources*, *188*(1), 14-23.

[25] Rostami, L., Nejad, P. M. G., & Vatani, A. (2016). A numerical investigation of serpentine flow channel with different bend sizes in polymer electrolyte membrane fuel cells. *Energy*, *97*, 400- 410.

[26] Bondue, C. J., Graf, M., Goyal, A., & Koper, M. T. (2020). Suppression of Hydrogen Evolution in Acidic Electrolytes by Electrochemical CO_2 Reduction. *Journal of the American Chemical Society*.

[27] Ooka, H., Figueiredo, M. C., & Koper, M. T. (2017). Competition between hydrogen evolution and carbon dioxide reduction on copper electrodes in mildly acidic media. *Langmuir*, *33*(37), 9307-9313.

[28] Raciti, D., Mao, M., & Wang, C. (2017). Mass transport modelling for the electroreduction of CO_2 on Cu nanowires. *Nanotechnology*, *29*(4), 044001.

[29] Wheeler, D. G., Mowbray, B. A., Reyes, A., Habibzadeh, F., He, J., & Berlinguette, C. P. (2020). Quantification of water transport in a CO_2 electrolyzer. *Energy & Environmental Science*, *13*(12), 5126-5134.

[30] Song, H., Song, J. T., Kim, B., Tan, Y. C., & Oh, J. (2020). Activation of C2H4 reaction pathways in electrochemical CO_2 reduction under low CO_2 partial pressure. *Applied Catalysis B: Environmental*, *272*, 119049.

[31] Jeon, D. H., Greenway, S., Shimpalee, S., & Van Zee, J. W. (2008). The effect of serpentine flow-field designs on PEM fuel cell performance. *International journal of hydrogen energy*, *33*(3), 1052-1066.

[32] Bohra, D., Chaudhry, J. H., Burdyny, T., Pidko, E. A., & Smith, W. A. (2019). Modeling the electrical double layer to understand the reaction environment in a CO_2 electrocatalytic system. *Energy & Environmental Science*, *12*(11), 3380-3389.

[33] Seifitokaldani, A., Gabardo, C. M., Burdyny, T., Dinh, C. T., Edwards, J. P., Kibria, M. G., & Sargent, E. H. (2018). Hydronium-induced switching between CO_2 electroreduction pathways. *Journal of the American Chemical Society*, *140*(11), 3833-3837.

[34] Gabardo, C. M., Seifitokaldani, A., Edwards, J. P., Dinh, C. T., Burdyny, T., Kibria, M. G., & Sinton, D. (2018). Combined high alkalinity and pressurization enable efficient CO_2 electroreduction to CO. *Energy & Environmental Science*, *11*(9), 2531-2539.

[35] Lu, X., Zhu, C., Wu, Z., Xuan, J., Francisco, J. S., & Wang, H. (2020). In situ observation of the pH gradient near the gas diffusion electrode of CO_2 reduction in alkaline electrolyte. *Journal of the American Chemical Society*, *142*(36), 15438-15444.